ESTIMATING TURBULENCE INTENSITY AND INTEGRAL SCALE IN THE NEAR REGION OF TURBULENCE GRIDS

Leah-Kathleen Lavoie
Department of Mechanical Engineering
McGill University
Montreal, Canada
leah-kathleen.lavoie@mail.mcgill.ca

Jovan Nedić
Department of Mechanical Engineering
McGill University
Montreal, Canada
jovan.nedic@mcgill.ca

ABSTRACT

We present a method by which the turbulence intensity and the integral scale can be predicted in the near region of decaying grid turbulence. The near region is defined as within 30 mesh lengths. A total of 13 different grids were investigated, spanning a wide range of mesh sizes, bar thickness, and grid solidity. The proposed scalings predict the turbulence intensity to, on average, an error of 3.4%, whilst errors of the integral scale are on average around 6.8%.

1 INTRODUCTION

Turbulence grids are a common tool used throughout experimental fluid dynamics to generate near-isotropic homogeneous turbulence. Besides their use for fundamental studies of decaying turbulence, they are also extensively used to generate turbulent conditions to study the effects of background turbulence on the flow around various bodies. Bearman (1971), for example, showed that the base pressure over square and circular plates in turbulent flow increased in the presence of background turbulence. Hoffmann (1991) demonstrated that background turbulence increases a finite wing's peak lift coefficient, as well as its drag coefficient. Vita *et al.* (2020) showed that the integral length scale determines the critical turbulence intensity ($\sim 5\%$) beyond which the coefficient of pressure surrounding an infinite wing would significantly change. The latter corroborates similar work by Bearman (1971) and Humphries & Vincent (1976), in that both the integral scale and turbulence intensity combined play an important role for bodies submerged in turbulent flows.

These studies demonstrate the importance, therefore, of being able to control both the integral scale and turbulence intensity when designing an experiment. Despite turbulence grids being used for over a century, it wasn't until the late 1980's that Roach (1987) provided the first comprehensive study, which attempted to provide the experimenter with a means of predicting the turbulence intensity and integral scale from grid design parameters. Combining data from a wide range of studies, Roach (1987) concluded that the turbulence intensity far downstream of bi-planar grids of diameter d is best modeled as

$$T_u = 1.13 \left(\frac{x}{d}\right)^{-5/7}. \tag{1}$$

Despite commenting on the fact that the constant of proportionality should depend on bar geometry and drag coefficient, a single value of 1.13 was applied to all the cases, even though there is clear scatter in the data. Note that this scaling was only applied for $x > 30M$, where M is the mesh size. Similarly, for the integral scale Λ, Roach (1987) observed that

$$\Lambda = 0.20 \left(\frac{x}{d}\right)^{1/2}. \tag{2}$$

Planar turbulence grids, as opposed to bi-planar grids, have grown in popularity over recent years with the advent of laser cutting technology. As these grids were not studied by Roach (1987), it is worthwhile verifying if Equations (1) and (2) hold for such grids. More importantly, we wish to investigate how the constants of proportionality in Equations (1) and (2) vary with grid geometry. Lastly, we also wish to investigate these scalings in the near region of decaying turbulence, where the turbulence intensity is known to be larger, but also decays faster.

2 THEORETICAL FRAMEWORK

Turbulence grids are defined by their mesh length (M), bar thickness (d), depth (t), and solidity $\sigma = \frac{d}{M}(2 - \frac{d}{M})$. A large body of work has shown that turbulence intensity downstream of grids decays as

$$T_u = A_M (x/M)^n \equiv A(x/d)^n . \tag{3}$$

Note that the decay rate is the same regardless of whether M or d are used; however, the constant of proportionality would be different. We will use the scaling with d such that a direct comparison to Roach (1987) can be made. If we assume that n is an approximately constant value, which Roach (1987) and several others have shown it to be, then one only needs to accurately model a single T_u value to estimate A. A reasonable candidate for this is the location, x_p, and the value of peak turbulence intensity, $T_{u,max}$. Following the scalings proposed by Gomes-Fernandes *et al.* (2012), we can approximate these as

$$x_p = \frac{M^2}{dC_D} \qquad T_{u,max} = \left(\frac{dC_D}{x_p}\right)^{0.5} . \tag{4}$$

Note here that $C_D = \mathrm{fn}(t,d)$ is the drag coefficient of infinite bars, the values of which can be obtained from Bearman & Trueman (1972). Inserting Equation (4) into Equation (3), we obtain an expression for the coefficient A

$$A = \left(\frac{d}{M}\right)^{2n+1} (C_D)^{n+1} . \tag{5}$$

We acknowledge that all three equations would have constants of proportionality, however, because the actual peak turbulence intensity is an inflection point in the curve, which a power law fit can not predict, we know, *apriori*, that our estimate of A will be inaccurate even if they were included. Instead, we will seek an empirical relation between this prediction of A, and those obtained from experiments, which we shall refer to as A^*. Finally, given the relation between T_u and Λ via the rate of turbulent kinetic energy dissipation, one can reasonably expect the equation for Λ_u to be closely linked to A. Similarly to T_u, Λ_u grows downstream following

$$\frac{\Lambda_u}{d} = B\left(\frac{x}{d}\right)^m \tag{6}$$

where m is the constant growth exponent and B is a proportionality constant. This work aims to define an empirical relation predicting values of B given the relation between T_u and Λ_u, with the assumption that $B = \mathrm{fn}(A)$.

The objective of this work is to predict both T_u and Λ_u in the near region of planar turbulence grids using the framework above. First, the values values obtained experimentally (A_{exp}) will be compared to their predicted values A (Equation (5)). A correction between experimental and predicted values will then be proposed using A^*. Finally, a framework to predict B_{exp} by using A^* will be given.

3 EXPERIMENTAL SETUP

All experiments were conducted with a bulk velocity $U_\infty \sim 5.6$ m/s in the low-speed Newman wind tunnel in the Aerodynamics Lab at McGill University. Planar mesh grids made of acrylic sheets with a thickness (t) of 6 mm were used. A total of 13 grids were investigated, the details of which are shown in Table 1. These grids cover a wide range of mesh sizes, solidity, as well as grid thickness t to bar thickness d ratios consequently giving a wide range of C_D values. For example, RG2035 with a mesh size of 2 in and a solidity of 35%, has the same bar thickness of $d = 0.39$ in and thus the same C_D as RG1545, which has a mesh of 1.5 in and a solidity of 45%.

Table 1: Planar turbulence generating grids used throughout experiments with their respective mesh length (M), bar thickness (d), grid solidity (σ), and drag coefficient (C_D).

Grid	M [mm/in]	d [mm/in]	σ	C_D	Symbol
RG4020	101.6/4.00	10.7/0.42	0.20	2.68	✻
RG4035	101.6/4.00	19.7/0.78	0.35	2.14	◆
RG4050	101.6/4.00	29.8/1.17	0.50	2.07	★
RG2020	50.8/2.00	5.36/0.21	0.20	1.98	✻
RG2025	50.8/2.00	6.81/0.27	0.25	2.34	●
RG2030	50.8/2.00	8.30/0.33	0.30	2.61	■
RG2035	50.8/2.00	9.84/0.39	0.35	2.93	◆
RG2040	50.8/2.00	11.5/0.45	0.40	2.52	◀
RG2045	50.8/2.00	13.1/0.52	0.45	2.32	▲
RG2050	50.8/2.00	14.9/0.59	0.50	2.23	★
RG1535	38.1/1.50	7.38/0.29	0.35	2.44	◆
RG1545	38.1/1.50	9.84/0.39	0.45	2.93	▲
RG1050	25.4/1.00	7.44/0.29	0.50	2.45	★

All measurements were obtained using cross-wire anemometry at 50 kHz with 25 repeats at 3 s each, with measurements taken along the grid's centerline over a distance of $0 \leq x \leq 1250$ mm downstream of each grid tested. Based on the mesh sizes listed in Table 1, this corresponds to a maximum range of $12.3 \leq (x/M)_{max} \leq 49.2$, or $42 \leq (x/d)_{max} \leq 233$.

4 RESULTS

Initially identifying the region defined by a power law decay (T_u) and growth (Λ_u) begins with identifying the point downstream after which the mean streamwise velocity $\overline{U}$ has become constant. Figure 1 shows the resulting mean streamwise velocity values downstream from each tested grid normalized by the bulk velocity U_∞ obtained via the streamwise velocity value furthest away from the grid. All grids eventually tend to $\overline{U} = U_\infty$ at varying distances downstream, after experiencing a high peak mean velocity as the flow is jetted through the grids' mesh. Grids with the highest mesh size (e.g., RG4020) reach bulk velocity much further downstream relative to their mesh size than with other tested grids, while smaller mesh grids (e.g. RG1050) tend to U_∞ much closer to the grid. Furthermore, for constant mesh grids, increasing the grids' σ results in $\overline{U}/U_\infty$ tending to 1 closer to the grid, with the exception of RG2045 and RG2050. The isotropy ratio $\sqrt{\overline{u^2}}/\sqrt{\overline{v^2}}$ is plotted in Figure 2. Values of 1.1 - 1.2, which are commonly accepted values for large-scale isotropy of turbulence grids, are achieved by all tested grids in a similar region to where the mean flow has achieved $\overline{U} = U_\infty$. Turbulence intensity (T_u) and integral length-scale (Λ_u) are shown in Figure 3. A distinct peak in T_u is observed for all grids, before decaying to a power-law relationship throughout the remainder of the measurement range. The location of the peak turbulence intensity for grids with the same solidity occur at the a similar x/d or x/M location. By increasing the solidity σ, the location of the peak intensity was found to move closer to the grid, as well as increasing the resulting turbulence inten-

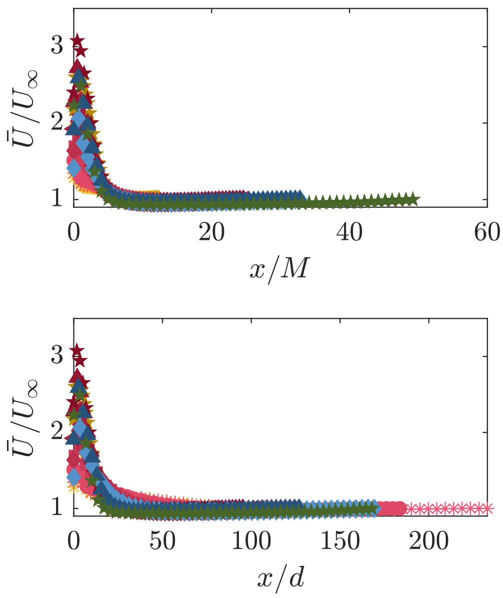

Figure 1: Mean streamwise velocity ($\overline{U}$) normalized by bulk velocity (U_∞). Symbols are defined as shown in Table 1.

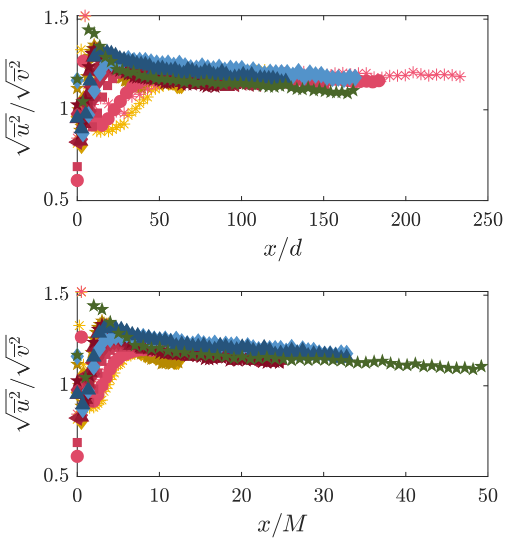

Figure 2: Streamwise variation of large-scale isotropy ratio $\sqrt{\overline{u}^2}/\sqrt{\overline{v}^2}$ for all tested grids.

sity at the peak. As for integral length-scale, for a given value fo M, Λ_u/d increases with decreasing solidity, whereas Λ_u/M increases with decreasing mesh length M. For both cases, increasing the value of M for a given σ results in a decrease to both Λ_u/d and Λ_u/M.

4.1 Predicting Turbulence Intensity

After isolating the power-law region using $\overline{U}/U_\infty$, Equation (3) is fitted to the T_u curves in Figure 3. While the x/d and x/M relationships are shown, the framework will be exclusively evaluated using x/d to compare with the results proposed by Roach (1987). Grid RG2040 will be used as an example and its resulting power-law is shown in Figure 4. While Roach (1987) proposed a $-5/7$ decay exponent far downstream, RG2040 in the near grid region exhibits a faster decay rate of -0.95 .

Table 2: Resulting decay exponent n for T_u fitted to Equation (3).

Grid	n	Symbol
RG4020	-0.59	✻
RG4035	-1.08	◆
RG4050	-1.23	★
RG2020	-0.87	✻
RG2025	-0.92	●
RG2030	-0.99	■
RG2035	-0.90	◆
RG2040	-0.95	◀
RG2045	-0.83	▲
RG2050	-1.01	★
RG1535	-0.79	◆
RG1545	-0.81	▲
RG1050	-0.73	★

Table 2 presents the resulting decay exponents of the turbulence intensity, n, for all tested grids. The majority of these grids exhibit different decay rates to that by Roach (1987) indicating that a new constant n should be proposed. The average value of all the resulting decay exponents is $n \approx -0.9$. This will be used as the decay rate for the near region of all planar grids. Figure 5 shows the resulting power-law fits using Equation (3) and $n = -0.9$ for the RG2040 sample case. The coefficient obtained using $n = -0.9$ shall be referred to as A_{exp}. For the example of the RG2040 case, this would mean that $A_{exp} = 3.09$. Recall that in our analysis we are only considering the case with the streamwise distance normalized by d so that a comparison can be done with Roach (1987). The resulting values of A_{exp} for all of the grids are shown in Table 4. In the same table, we show the value of A using Equation (5) with $n = -0.9$. For most cases, $A < A_{exp}$; however, the values of A are in good qualitative agreement with A_{exp}. We also note that for constant M, increasing the solidity results in a decrease to A_{exp}, which is captured well using the approximation A.

To obtain a better prediction of A_{exp} using A, both values are plotted against each other in Figure 6. Although there is some scatter, a clear relationship exists between A_{exp} and A, with a correlation coefficient $\rho = 0.968$. Fitting a power-law function to A_{exp} as a function of A gives the following relationship

$$A^* = 1.82A^{0.43}, \tag{7}$$

where A^* is now the best fit constant of proportionality for all the grids, based on our assumption of Equation (5). A^* for all grids tested are outlined in Table 5.

Following the example of RG2040, $A^* = 3.15$ which is a much closer approximation of $A_{exp} = 3.09$ than the original es-

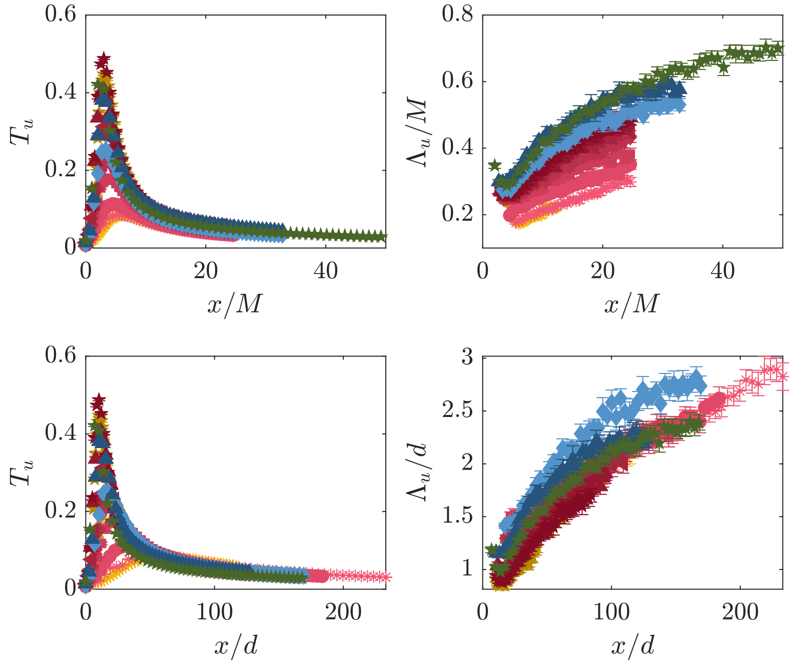

Figure 3: Turbulence intensity (T_u) and integral length scale (Λ_u) as a function of x.

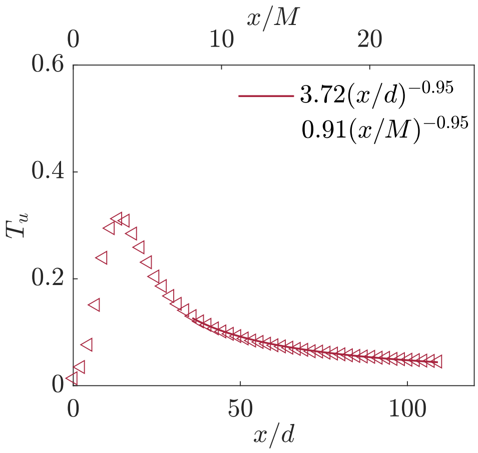

Figure 4: T_u of RG2040 fitted to Equation (3).

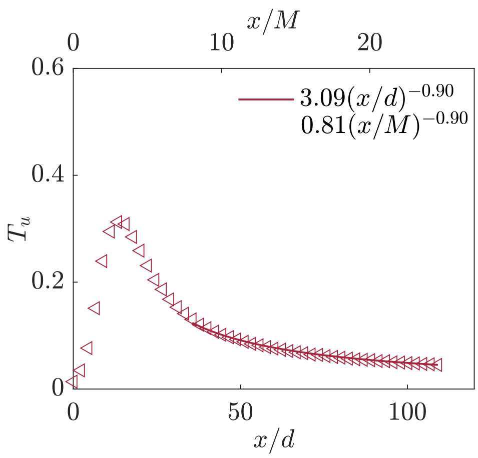

Figure 5: Power-law fit using equation (3) and constant decay exponent $n = -0.9$ for RG2040.

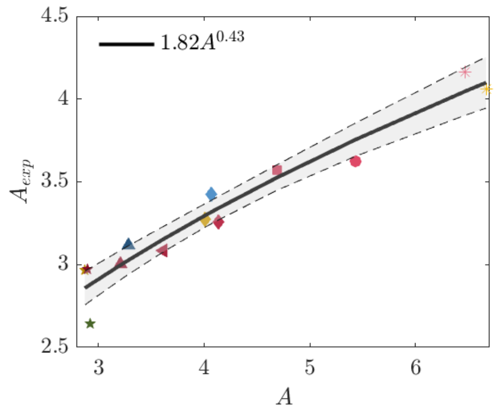

Figure 6: A_{exp} as a function of its theoretical value A determined by Equation (5) using $n = -0.9$.

timate $A = 3.61$. Combining Equation (3), with Equation (5) and Equation (7), and setting $n = -0.9$, the following equation for the variation of streamwise turbulence intensity with downstream distance, once the flow have achieved $\overline{U} = U_\infty$, is obtained:

$$T_u = 1.82\left[\left(\frac{d}{M}\right)^{-0.8}(C_D)^{0.1}\right]^{0.43}\left(\frac{x}{d}\right)^{-0.9}. \tag{8}$$

4.2 Predicting Integral Length-Scale

The same method is used for the integral scale. First, we must find m from Equation (6), the values of which are shown in Table 3. For our example case of the RG2040 grid, $m = 0.35$, and the resulting least-square fit is shown in Figure 7. Note that all of the values of m in Table 3 are lower than the 0.5 used by Roach (1987). Taking the average value of m from

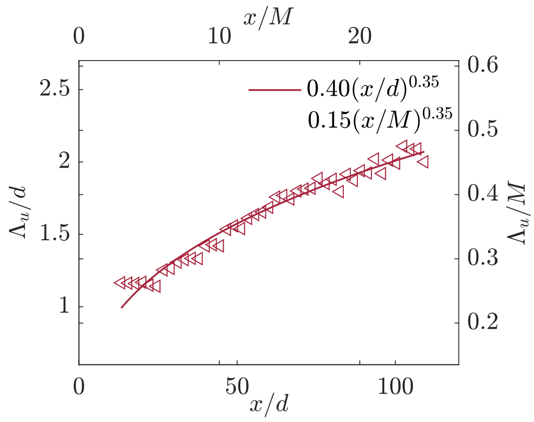

Figure 7: Λ_u/d fitted to Equation (6) for RG2040

Table 3: Resulting decay exponent n for T_u fitted to equation (3).

Grid	m	Symbol
RG4020	0.37	✻
RG4035	0.20	◆
RG4050	0.29	★
RG2020	0.38	✻
RG2025	0.31	●
RG2030	0.29	■
RG2035	0.34	◆
RG2040	0.35	◀
RG2045	0.38	▲
RG2050	0.39	★
RG1535	0.32	◆
RG1545	0.31	▲
RG1050	0.33	★

Table 3 gives $m \approx 3/8$, which will be used for the remainder of our analysis. Using this m, values of B_{exp} can be defined. For example, RG2040 shown in Figure 8 has $B_{exp} = 0.36$ with a growth rate of $m = 3/8$. All values of B_{exp} are presented in Table 4.

Given our assumption that $B = \mathrm{fn}(A)$, as mentioned in Section 1, it also holds that $B = \mathrm{fn}(A^*)$, given that $A^* = \mathrm{fn}(A)$. From Table 4, we also observe that $B_{exp} = \mathrm{fn}(\sigma)$, in that it decreases as solidity increases for a constant mesh size M. We therefore plot B_{exp}/σ as a function of A^* in Figure 9, where a clear trend is observed, namely

$$\frac{B}{\sigma} = 0.04A^{*2.73}\,, \tag{9}$$

with a correlation coefficient of $\rho = 0.987$. All values of B are shown in Table 5. Again returning to our sample case of RG2040, the predicted value for B_{exp} is $B = 0.36$, which

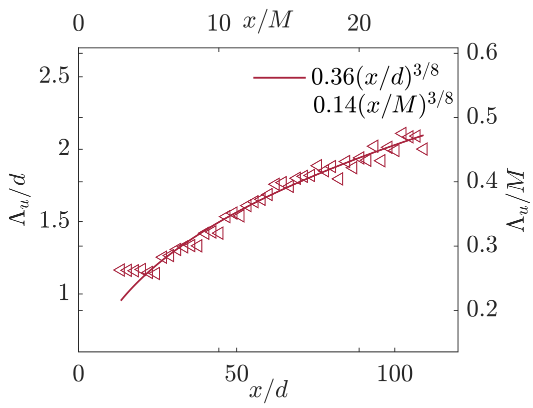

Figure 8: Λ_u/d fit to Equation (6) using $m = 3/8$.

Table 4: Experimental values A_{exp} using $n = -0.9$ compared to predicted values A using Equation (5). As well, experimental values B_{exp} obtained using $m = 3/8$.

Grid	A_{exp}	A	B_{exp}	Symbol
RG4020	4.06	6.67	0.36	✻
RG4035	3.27	4.01	0.34	◆
RG4050	2.97	2.87	0.30	★
RG2020	4.16	6.47	0.37	✻
RG2025	3.63	5.44	0.37	●
RG2030	3.57	4.69	0.37	■
RG2035	3.26	4.14	0.37	◆
RG2040	3.09	3.61	0.36	◀
RG2045	3.00	3.21	0.34	▲
RG2050	2.97	2.89	0.32	★
RG1535	3.42	4.06	0.43	◆
RG1545	3.12	3.29	0.40	▲
RG1050	2.64	2.92	0.37	★

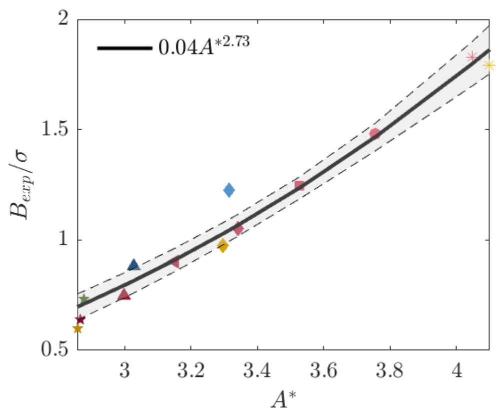

Figure 9: B_{exp}/σ as a function of A^* obtained using Equation (7).

Table 5: Investigated planar grids, together with their design parameters, and average percentage error to the data for the given fits.

Grid	A^*	B	$\overline{\varepsilon_{Tu}}$ [%] Equation (8)	$\overline{\varepsilon_{Tu}}$ [%] Equation (1)	$\overline{\varepsilon_{\Lambda}}$ [%] Equation (10)	$\overline{\varepsilon_{\Lambda}}$ [%] Equation (2)
RG4020	4.10	0.37	4.46	45.01	3.99	2.69
RG4035	3.30	0.36	2.10	31.91	7.55	2.48
RG4050	2.86	0.35	5.05	29.86	14.49	4.32
RG2020	4.05	0.36	3.09	35.53	2.36	3.93
RG2025	3.76	0.37	3.72	26.88	2.85	4.03
RG2030	3.53	0.37	2.59	28.99	3.82	6.88
RG2035	3.34	0.37	2.47	21.77	2.89	4.00
RG2040	3.15	0.36	3.00	21.09	2.89	6.04
RG2045	3.00	0.36	1.27	18.46	6.47	2.07
RG2050	2.87	0.35	2.24	21.72	9.88	3.27
RG1535	3.32	0.36	3.49	19.21	17.08	12.03
RG1545	3.03	0.37	4.29	20.61	9.30	12.77
RG1050	2.88	0.35	6.18	0.65	5.08	5.32

matches B_{exp}. Combining all of the above, a prediction for the streamwise variation of Λ_u/d throughout the near grid region of a turbulence grid, with the condition that $\overline{U} = U_\infty$, is

$$\frac{\Lambda_u}{d} = 0.04 \left\{ 1.82 \left[\left(\frac{d}{M} \right)^{-0.8} (C_D)^{0.1} \right]^{0.43} \right\}^{2.73} \left(\frac{x}{d} \right)^{3/8}. \tag{10}$$

4.3 Error Comparison

Given Equation (8) and Equation (10), an average percentage error between the fit and the measured value can be obtained for each grid. These values are shown in Table 5, where $\overline{\varepsilon_{Tu}}$ is the average fit error for the turbulence intensity, and $\overline{\varepsilon_{\Lambda}}$ is the average fit error for the integral scale. The corresponding errors for the fits of Roach (1987) are also shown. For the turbulence intensity, it is clear that Roach (1987) drastically overestimates T_u in the near grid region, whereas Equation (8) produces lower errors, with an average error of 3.4% across all the grids considered here. The prediction of the integral scales, on the other hand, are similar in terms of their average error, with an average error of 6.8% based on Equation (10).

5 CONCLUSION

This work presented a framework for predicting values of T_u and Λ_u using Equation (8) and Equation (10), which are in turn based on design parameters of the turbulence grid. The proposed fits are only valid for regions where $\overline{U} = U_\infty$, and have only been tested in the near-region of turbulence grids, namely for $x < 30M$. Overall, the error when using these methods remained low, with the error in turbulence intensity having an average value of 3.4%, and the average error in the integral scale of 6.8%. These errors are a significant improvement on the previously proposed fits by Roach (1987). Future work will focus on exploring how the fits can be used to better predict the location of the peak turbulence intensity, as well as its value, as well as providing equivalent expressions for Equation (8) and Equation (10) using x/M.

REFERENCES

Bearman, PW 1971 An investigation of the forces on flat plates normal to a turbulent flow. *Journal of Fluid Mechanics* **46** (1), 177–198.

Bearman, PW & Trueman, DM 1972 An investigation of the flow around rectangular cylinders. *Aeronautical Quarterly* **23** (3), 229–237.

Gomes-Fernandes, R, Ganapathisubramani, B & Vassilicos, JC 2012 Particle image velocimetry study of fractal-generated turbulence. *Journal of Fluid Mechanics* **711**, 306–336.

Hoffmann, Jon A 1991 Effects of freestream turbulence on the performance characteristics of an airfoil. *AIAA journal* **29** (9), 1353–1354.

Humphries, W & Vincent, JH 1976 Experiments to investigate transport processes in the near wakes of disks in turbulent air flow. *Journal of Fluid Mechanics* **75** (4), 737–749.

Roach, PE 1987 The generation of nearly isotropic turbulence by means of grids. *International Journal of Heat and Fluid Flow* **8** (2), 82–92.

Vita, G, Hemida, H, Andrianne, T & Baniotopoulos, C 2020 The effect of the integral length scale of turbulence on a wind turbine aerofoil. *Journal of Wind Engineering and Industrial Aerodynamics* **204**, 104235.